

# Latitudinal variation of the effect of aviation NO<sub>x</sub> emissions on atmospheric ozone and methane and related climate metrics

M. O. Köhler<sup>a,c,\*</sup>, G. Rädcl<sup>b,d</sup>, K. P. Shine<sup>b</sup>, H. L. Rogers<sup>a</sup>, J. A. Pyle<sup>a</sup>

<sup>a</sup>*Centre for Atmospheric Science, Department of Chemistry, University of Cambridge, UK*

<sup>b</sup>*Department of Meteorology, University of Reading, UK*

<sup>c</sup>*now at Department of Geography, King's College London, UK*

<sup>d</sup>*now at Max-Planck-Institute for Meteorology, Hamburg, Germany*

---

## Abstract

We evaluate the response to regional and latitudinal changes in aircraft NO<sub>x</sub> emissions using several climate metrics (radiative forcing (RF), global warming potential (GWP), global temperature change potential (GTP)). Global chemistry transport model integrations were performed with sustained perturbations in regional aircraft and aircraft-like NO<sub>x</sub> emissions. The RF due to the resulting ozone and methane changes is then calculated. We investigate the impact of emission changes for specific geographical regions (approximating to USA, Europe, India and China) and cruise altitude emission changes in discrete latitude bands covering both hemispheres. We find that lower latitude emission changes (per Tg N) cause ozone and methane RFs that are about a factor of 6 larger than those from higher latitude emission changes. The net RF is positive for all experiments. The meridional extent of the RF is larger for low latitude emissions. GWPs for all emission changes are positive, with tropical emissions having the largest values; the sign of the GTP depends on the choice of time horizon.

*Keywords:* Aircraft emissions, Nitrogen oxides, Greenhouse gases, Radiative forcing, Climate metrics

---

---

\*Corresponding author. Department of Geography, King's College London, Strand, London, WC2R 2LS, United Kingdom.

*Email address:* [marcus.koehler@kcl.ac.uk](mailto:marcus.koehler@kcl.ac.uk) (M. O. Köhler)

## 1. Introduction

Emissions from global aviation alter atmospheric composition. These emissions include oxides of nitrogen ( $\text{NO}_x = \text{NO} + \text{NO}_2$ ) which result in the increased formation of ozone ( $\text{O}_3$ ) and in a reduced lifetime and concentration of methane ( $\text{CH}_4$ ) (see Lee et al., 2010; Myhre et al., 2011; Holmes et al., 2011, and references therein) and result in a radiative forcing (RF) that can drive climate change. The RF due to  $\text{NO}_x$  emissions depends sensitively on where the emissions occur unlike emissions of carbon dioxide ( $\text{CO}_2$ ) which is long lived and hence globally well-mixed.

Air traffic has a heterogeneous global distribution with the majority concentrated in northern hemisphere mid-latitudes, particularly over North America, Europe, the North Atlantic and Japan (Eyers et al., 2005). A substantial increase in future air traffic is predicted in countries with fast growing economies such as China and India (ACI, 2011).

We investigate the link between the location of aircraft  $\text{NO}_x$  emissions and the consequent RF, by examining the effect of emissions from four distinct regions: Two of these experience high air traffic today; in the other two air traffic is expected to grow significantly. We also examine systematically the effect of latitude of aircraft emissions at cruise altitude. We apply sustained regional perturbations to aircraft  $\text{NO}_x$  emissions from a contemporary emissions inventory, using a global chemistry transport model in combination with an off-line radiative transfer model. We then calculate climate emission metrics (the Global Warming Potential and Global Temperature Change Potential) to illustrate the dependence on the type of climate metric.

A particular difficulty is that the net RF of  $\text{NO}_x$  emissions is a residual of effects of opposing signs – a short-lived and positive ozone RF directly resulting from the  $\text{NO}_x$  emissions is accompanied by a longer-lived negative forcing due to a consequent decrease in methane concentrations and an associated decrease in ozone. Further impacts from  $\text{NO}_x$  emissions are the formation of nitrate particles (Kärcher, 1996) and indirectly a more effective conversion of  $\text{SO}_2$  to sulphuric acid due to an increase in OH and the subsequent formation of sulphate aerosol (Pitari et al., 2002). These further  $\text{NO}_x$  impacts have been much less studied and are not considered here.

The net RF from aircraft  $\text{NO}_x$  emissions for the year 2005 is reported by Lee et al. (2010) as the second largest ( $13.8 \text{ mW m}^{-2}$ ) after that from  $\text{CO}_2$  ( $28 \text{ mW m}^{-2}$ ). The more uncertain RF for aircraft-induced cloudiness could however be larger than these (estimated  $33 \text{ mW m}^{-2}$ ). Hoor et al.

(2009), Myhre et al. (2011) and Holmes et al. (2011) report large inter-model differences in the RF of aircraft  $\text{NO}_x$ . The relative importance of aircraft  $\text{NO}_x$  is influenced by the background  $\text{NO}_x$  concentrations, originating from surface or lightning emissions (Berntsen and Isaksen, 1999). The abundance of the oxides of hydrogen ( $\text{HO}_x$ ), volatile organic compounds (VOCs), as well as the available solar irradiance play further important roles (Jaeglé et al., 1998a). Earlier modelling studies (e.g. Berntsen et al., 2005; Derwent et al., 2008) found that the global-mean RF and surface temperature change resulting from surface  $\text{NO}_x$  emissions depend on where emissions occur. Köhler et al. (2008) have shown that changing the flight routing pattern at cruise altitudes significantly changes the impact on ozone and methane, and the associated RF. Grewe and Stenke (2008) found a significant difference in the RF from aircraft  $\text{NO}_x$  emissions in four latitude bands and six height levels for a 2050 background scenario. Stevenson and Derwent (2009) calculated the effect of location of cruise-level aviation  $\text{NO}_x$  emissions on the 100-year time-integrated RF (the absolute global warming potential) in response to pulse emissions of  $\text{NO}_x$  in about 100 different locations. They show a strong dependence on the background  $\text{NO}_x$  levels, and emphasise the compensation between the short-lived ozone effect and the longer-lived methane effect.

We quantify here the effect of the location of aircraft  $\text{NO}_x$  emissions on RF by increasing  $\text{NO}_x$  emissions by small amounts in different regions and at different latitudes. This will illustrate how the effect of aviation  $\text{NO}_x$  emissions on ozone, methane, and the associated RF depend on the location of emissions, which is of particular importance as future growth in aviation emissions is likely to be globally heterogeneous. The results for metrics have potential applications in policy contexts (see e.g. Fuglestvedt et al., 2010) and when considering the climate impact of changes in aircraft design (e.g. Schwartz Dallara et al., 2011).

Sections 2 and 3 describe the model and experiment setup. Section 4 focuses on composition changes and the associated RF. Section 5 presents the climate metrics. We conclude with a discussion of our findings.

## 2. Model Description

The p-TOMCAT chemistry transport model was used in a similar configuration as in Hoor et al. (2009) and Myhre et al. (2011), an updated version compared with that used in Köhler et al. (2008); the most important updates concern the model's chemical reaction rates and surface emissions. As

in Hoor et al. (2009) the model grid has a horizontal resolution of  $5.6 \times 5.6$  degrees, but with increased vertical resolution of 35 vertical levels between the surface and 10 hPa as in Köhler et al. (2008) resulting in a vertical grid spacing of approximately 700 m in the upper troposphere and lower stratosphere (UTLS). Horizontal tracer advection was calculated by conservation of second-order moments (Prather, 1986). Vertical transport was based on the Tiedtke (1989) convective mass flux parameterization and a non-local vertical diffusion scheme (Holtslag and Boville, 1993). Lightning  $\text{NO}_x$  emissions are linked to the convection scheme (Stockwell et al., 1999) and scaled to a total of  $5 \text{ Tg (N) yr}^{-1}$ . A more detailed model description is given in Cook et al. (2007) and Hoyle et al. (2011). The chemistry is as described in Hoor et al. (2009) with the exception that our study does not include homogeneous and heterogeneous sulphur chemistry. Chemical reaction rates were consistent with Atkinson et al. (2005) and JPL (2003) resulting in a methane lifetime of 7 years with respect to all losses. The shorter  $\text{CH}_4$  lifetime compared to that in Köhler et al. (2008) is due to the models updated surface emissions and chemical reaction rates. The model integrations were forced by analyses from the European Centre for Medium-Range Weather Forecasts for 2001 and 2002. 2001 served as a spin-up period to allow the model to reach steady-state with regard to the sustained emission perturbation in each experiment. Only model results for 2002 are presented. As described in Hoor et al. (2009) the surface emissions were based on the Emission Database for Global Atmospheric Research (EDGAR) 32FT2000 inventory (van Aardenne et al., 2005; Olivier et al., 2005). Methane however was globally fixed at 1820 ppbv for the northern hemisphere (NH) and 1720 ppbv southern hemisphere (SH). Road traffic emissions in EDGAR were replaced by Borcken and Steller (2006) and shipping emissions by Endresen et al. (2007). Aircraft  $\text{NO}_x$  emissions for 2002 were taken from the AERO2k inventory (Eyers et al., 2005). A breakdown of the individual non-aviation emissions is shown in Table 1 of Hoor et al. (2009). p-TOMCAT does not include a sub-grid scale parameterization for emissions (c.f. Meijer et al., 1997) and thus we expect the diagnosed chemical response in the results to be slightly overestimated due to the instantaneous mixing of the emitted  $\text{NO}_x$ .

RFs due to ozone changes from  $\text{NO}_x$  emissions were calculated using the Edwards-Slingo radiation code (Edwards and Slingo, 1996), an offline version of the code used in the UK Met Office Unified Model. It uses the  $\delta$ -Eddington approximation in the solar region of the spectrum. Spectral resolutions were six bands in the shortwave and eight bands in the longwave.

Stratospheric adjustment was calculated using the fixed dynamical heating approximation (Ramanathan and Dickinson, 1979). Climatological cloud amounts were taken from Rossow and Schiffer (1991). RF calculations were performed using monthly-mean ozone perturbations from p-TOMCAT (we refer to this as the short-lived ozone forcing). In the case of the latitudinal-band perturbations described below, the ozone perturbations were multiplied by a factor 100 to avoid numerical problems with small forcing values. The resulting RFs were then divided by 100. The radiation code used here differs from that used in Köhler et al. (2008) but it was found that for the short-lived ozone forcing both codes agreed within about 10 percent. The methane RF follows the same simplified procedure described in Myhre et al. (2011) as it is not practicable to run the model for long enough for methane to come into equilibrium with the OH changes. We apply a commonly used method (explained in Fuglestvedt et al. (1999) and used in Köhler et al. (2008) and elsewhere) wherein the steady state methane changes are based on changes in the OH fields, multiplied by a multi-model average feedback factor of 1.4 to account for the effect of methane changes on its own lifetime. The methane specific RF is taken to be  $0.37 \text{ mW m}^{-2} \text{ ppbv}^{-1}$ . As in Myhre et al. (2011) this forcing is enhanced by 15% to account for the effect of methane change on stratospheric water vapour concentrations. Unless otherwise indicated, the methane forcing presented here incorporates the stratospheric water vapour forcing. The effect of the methane change on ozone (called the methane-induced ozone change here) is computed from multi-model averages whereby a 10% change in methane leads to a 0.64 DU change in ozone, with a specific RF of ozone of  $42 \text{ mW m}^{-2} \text{ DU}^{-1}$ .

We assume that the methane concentration change (and the consequent methane-induced ozone change) is in equilibrium with the change in OH due to the  $\text{NO}_x$  emission change. Hence our results represent the forcing several decades after the emission change. This differs from the RFs presented in Myhre et al. (2011) which were specifically for the year 2000, and included a simplified representation of the imbalance. The steady-state assumption (also used in Holmes et al., 2011) was more appropriate for the more idealized calculations presented here.

### 3. Experiments

We have carried out sensitivity studies where in one region at a time small perturbations in  $\text{NO}_x$  are applied. Emission scaling has been used

previously to estimate the contribution from individual sectors to changes in composition and RF (e.g., Hoor et al., 2009; Myhre et al., 2011). Critical evaluation of this method (e.g., Wang et al., 2009; Grewe et al., 2010) has raised concerns about non-linearities in the atmospheric response which can introduce uncertainties when large scaling factors are used. Grewe et al. (2010) and Myhre et al. (2011) however found that the non-linear response is small, especially when compared to inter-model differences; they conclude that emission scaling using small increments contributes little to the overall uncertainty.

We present results from two experiment groups. In the first group of four experiments (“Regional Perturbations”) aircraft  $\text{NO}_x$  emissions were increased at all altitudes in a limited domain. The domains are shown as rectangular boxes in the left column of Figure 1 and described in Table 1. They represent approximately the contiguous United States (USA), Europe, the Indian subcontinent, and the eastern part of China. The USA and Europe represent areas with mature air traffic infrastructure; India and China represent areas where strong growth is expected during the coming decades (ACI, 2011). The emissions increase was implemented by scaling the vertical aircraft  $\text{NO}_x$  emissions profile in the p-TOMCAT grid boxes located within each region by a constant factor. This factor was adjusted for each region such that the emission mass increase was equal to a 20% emissions increase over the USA region. This corresponds to additional emissions of 0.036 Tg (N) per year, and relative increases in Europe, China and India, of 28%, 108% and 260% respectively (see Table 1). Market forecasts for 2010–2029 (Airbus, 2010; Boeing, 2010) predict air traffic growth rates in revenue-passenger-km (RPK) per annum of 3.3–3.4% for North America, 4.1–4.4% for Europe and 5.8–6.8% for the Asia-Pacific region. Although aircraft emissions have not grown proportionally to the growth in RPK due to increasing aircraft efficiency, we still consider the increases in our experiments to be within the expected range for the coming decades in the absence of radical changes in operational practices or aircraft technology.

The second group of experiments (“Latitude Bands”) aims to establish to what extent the RF due to  $\text{NO}_x$  emissions at cruise altitude is a function of latitude. A fixed rate of emission of  $\text{NO}_x$  was equally distributed (independent from flight routing) in 20 degree latitude bands on three vertical model levels in the UTLS. This is compared with a reference experiment using the unaltered AERO2k  $\text{NO}_x$  emissions. Figure 2 shows the location of the latitude bands superimposed over the p-TOMCAT  $\text{NO}_x$  background mixing

ratios. The additional amount of  $\text{NO}_2$  emitted in each latitude band was the equivalent of 1% of aircraft emissions within the 40–60°N band (additional  $3.8 \cdot 10^{-4}$  Tg (N)  $\text{yr}^{-1}$ ). The amount was chosen to be small to minimise non-linear chemical effects (c.f. Köhler et al., 2008) and to make ozone and methane changes comparable through normalisation, as the surface area of individual latitude bands varies by approximately 30%.

## 4. Results

In p-TOMCAT the unaltered AERO2k  $\text{NO}_x$  emissions (0.68 Tg (N)  $\text{yr}^{-1}$ ) cause an increase in the global annual mean  $\text{O}_3$  column by 0.57 DU which is approximately 30% less than the change reported in Köhler et al. (2008). This reduction is caused by the inclusion of updated chemistry and surface emissions in the model. The all-sky global-mean stratospheric temperature adjusted RF from short-lived ozone was  $19.6 \text{ mW m}^{-2}$  (compared to  $22.7 \text{ mW m}^{-2}$  for the instantaneous forcing). Köhler et al. (2008) found a higher global RF ( $30 \text{ mW m}^{-2}$  for the same emissions) mainly due to the larger ozone changes in the previous calculations. Our new value corresponds to  $34 \text{ mW m}^{-2} \text{ DU}^{-1}$  which compares well with Myhre et al. (2011) who present an average value of  $36 \text{ mW m}^{-2} \text{ DU}^{-1}$  from five chemistry transport models, employing a different aircraft emissions inventory. In our study the aircraft  $\text{NO}_x$  emissions reduce the methane lifetime by 0.068 years. The ozone, methane (without stratospheric water vapour) and methane-induced ozone RFs normalised by  $\text{NO}_x$  emissions are 28.8,  $-14.4$  and  $-6.03 \text{ mW m}^{-2}$  per Tg (N) per year, respectively. These are in good agreement with the corresponding multi-model means of  $27.3 \pm 9.7$ ,  $-16.1 \pm 5.6$  and  $-6.6 \pm 3.3 \text{ mW m}^{-2}$  per Tg (N) per year given by Holmes et al. (2011). The net RF is  $8.4 \text{ mW m}^{-2}$  per Tg (N) per year (or  $6.3 \text{ mW m}^{-2}$  per Tg (N) per year when including stratospheric water vapour forcing), which is within the range of the very uncertain net value of  $4.5 \pm 4.5 \text{ mW m}^{-2}$  per Tg (N) per year range given in Holmes et al. (2011).

### 4.1. Regional Perturbations

The  $\text{NO}_x$  perturbations in the four regions show significant differences in their impacts on global  $\text{O}_3$  column and methane lifetime (Tables 1 and 2). The fourth column in Table 1 shows the extent to which the unaltered AERO2k aircraft emissions (without added perturbation) increase background  $\text{NO}_2$  levels at cruise altitude (10–12 km); the relative contribution is largest

over Europe and smallest over India. Emission increases over India and China lead to column  $O_3$  increases which are approximately a factor of two higher than over the USA and Europe. We suggest that a large contributor to this difference is the higher level of solar irradiance at lower latitudes which results in faster photochemical production of ozone. Further contributing factors may be differences in  $HO_x$  and VOCs abundances.

Meridional transport of  $O_3$  is more pronounced in perturbations at lower latitudes where  $NO_x$  emission changes affect  $O_3$  column over a larger geographical area (Fig. 1). Emission perturbations in the mid-latitudes, e.g. in the USA and China, are picked up by the prevalent westerlies and the associated peak  $O_3$  changes occur over the North Atlantic and over large parts of the central Pacific, respectively.  $NO_x$  emission increases over India result in peak  $O_3$  increases over the north-eastern Indian Ocean with a large seasonal effect depending on the monsoon phase (not shown). The vertical extent of the  $O_3$  change is larger for USA emissions compared with European emissions, and is still larger for emissions from China, and largest for emissions from India where strong convection leads to a chemical impact throughout the depth of the troposphere. Convective transport to higher altitude also results in a longer lifetime of the emitted  $NO_x$  as well as of the additional ozone produced by the  $NO_x$  perturbation. The impact of the  $NO_x$  perturbations on the methane lifetime (Table 2 final column) is more negative at low latitudes, with the largest effect found for emissions from India because of the larger change in ozone for these emissions. Output from p-TOMCATs chemical reaction channels, investigated by Köhler et al. (2008), has shown that the additional  $O_3$  produced from the  $NO_x$  increase results, through OH radical production, in a  $CH_4$  loss which is most efficient at low latitudes and low altitude, resulting in the  $CH_4$  lifetime reduction.

Figure 3 shows the methane lifetime change and the net global annual-mean RF, and the three component forcings, for the regional experiments. Table 2 presents the specific RFs (per Tg (N)  $yr^{-1}$ ). The net RF is shown by the black cross in the upper figure panel; its highest value is  $0.51 \text{ mW m}^{-2}$  for emission perturbations in China. While the short-lived  $O_3$  RF is largest for the India perturbation experiment ( $1.63$  compared to  $1.46 \text{ mW m}^{-2}$  in China) the methane and methane-induced ozone RFs play a relatively larger role there and reduce the net RF to  $0.45 \text{ mW m}^{-2}$ . The experiments for perturbations over the USA and Europe respectively, show much smaller short-lived  $O_3$  RFs ( $0.72$  and  $0.49 \text{ mW m}^{-2}$ ). This difference in RF between mid-latitude and (sub)-tropical latitudes is larger than the difference seen in

the  $O_3$  changes (Table 1) and is even larger for the net RFs (Table 2). For example, for the experiments over India and Europe the ratio of  $O_3$  changes is 2.3, the ratio of short-lived  $O_3$  induced RFs is 3.3, and the ratio of the net RFs is 5.9. Hence, the methane and methane-induced ozone changes are more effective at compensating the short-lived ozone RF for the two high-latitude experiments. These balances are subtle – Tables 1 and 2 indicate that the methane lifetime change per unit ozone change is almost invariant of the emission region (varying between 0.18 and 0.22 yr DU<sup>-1</sup>). The variation in ozone change per unit NO<sub>x</sub> emission, and the resulting specific forcing, drive the regional differences in the net forcing.

Figure 3 (middle panel) shows the latitudinal dependence of the RF due to the  $O_3$  increase. It reflects the effect described above and shown in Figure 1, that for emissions at lower latitudes (China and India) the RF is larger with the peak located near the latitudes of emission. Additional NO<sub>x</sub> emissions at higher latitudes like USA or Europe result in an overall smaller RF with its maximum at lower latitudes than the emissions. Hence, the latitude of the region is the driving factor for these different composition and forcing effects, such that the same amount of NO<sub>x</sub> emissions results in RFs that are larger when released at lower latitudes. This is consistent with similar experiments for surface NO<sub>x</sub> emissions (e.g. Berntsen et al., 2005). The experiments described in the next section provide further evidence.

#### 4.2. Latitude Bands

Figure 2 shows the zonal-mean annually averaged NO<sub>x</sub> distribution in p-TOMCAT for 2002, representing the NO<sub>x</sub> background to which emission increases are applied. The eight regions where emissions are increased are shown as boxes indicating their vertical and meridional extent. Emissions were increased at all longitudes in each of the eight boxes individually. At high latitudes (> 40°N or S) the additional NO<sub>x</sub> emissions are released mainly above the tropopause; at lower latitudes the perturbation is below the tropopause.

NO<sub>x</sub> levels increase sharply with altitude near the tropopause. Such gradients are difficult to reproduce accurately in global models, mainly due to insufficient vertical resolution. In general, atmospheric models tend to underestimate upper tropospheric NO<sub>x</sub> levels (Brunner et al., 2003; Henderson et al., 2011) due to the complex inter-related chemical and physical processes which govern transport and the partitioning of the reactive nitrogen compounds. Stratospheric influx, convective uplift from the lower troposphere

and lightning emissions (Berntsen and Isaksen, 1999) are important in determining upper tropospheric  $\text{NO}_x$  levels and, as sub-grid scale processes, they represent challenges for global models. Henderson et al. (2011) have investigated photochemical ageing of  $\text{NO}_x$  and reported wide-spread overestimation of  $\text{NO}_x$  to  $\text{HNO}_3$  conversion in models. Validation with satellite data (Savage et al., 2004) found that the TOMCAT model reproduced observed  $\text{NO}_x$  levels and their seasonal cycle reasonably well, although it underestimated upper tropospheric  $\text{NO}_x$ . A comparison with in-situ aircraft observations (Brunner et al., 2003) showed that the UTLS model bias varied between  $-10\%$  to  $-50\%$ . Other models in that study showed a similar bias.

The methane lifetime change and the resulting net global annual-mean RF, as well as the three component forcings, for each latitude experiment are shown in Figure 4. Table 2 presents the specific RF values. Figure 4 (top panel) shows a strong latitudinal dependence of the short-lived  $\text{O}_3$  RFs which is again a combination of the latitudinal variation in ozone production efficiency per  $\text{NO}_x$  molecule and their associated RFs per DU of ozone change. The largest ozone column increase is found for low latitude perturbations (bottom panel, Fig. 4), partly due to the relatively low  $\text{NO}_2$  background concentrations in the upper troposphere (c.f. Fig. 2) and partly due to higher insolation and higher ozone production rate. This is also reflected in the high short-lived ozone forcing at low latitudes. Figure 4 (middle panel) shows that for perturbations at latitudes higher than 40 degrees the ozone RF change is largely confined to the hemisphere of emission. For perturbations at  $20\text{--}40^\circ$  the peak ozone column increase is found largely over the oceans where background  $\text{NO}_x$  concentrations are lower (not shown). The compensating methane and methane-induced RF will be more globally distributed than the short-lived ozone forcing; hence the compensation between the global mean forcings will not necessarily be found on smaller scales.

Figure 4 (bottom panel) shows the impact on the global ozone column and methane lifetime change. While our figures show annual-mean results we diagnose the strongest seasonal change at high latitudes with virtually all ozone column increase occurring during polar day. In the inner-tropical region on the other hand the location of the inter-tropical convergence zone controls where the area with strongest ozone increase is found. The global-mean net forcing as a function of the latitude of emission is quasi-symmetric relative to the equator with large impacts at low latitudes and smaller impacts near the poles. However the impact both on ozone increase and methane lifetime reduction is larger for SH perturbations and weighted by the ozone

increase the impact on the methane lifetime is again larger in the SH. This is attributed to the lower  $\text{NO}_x$  background resulting in a larger sensitivity with respect to an emissions change.

As with the composition changes, the RFs due to emissions at a given SH latitude are larger than those for perturbations at the corresponding northern latitude. The smallest inter-hemispheric difference is observed for the  $20^\circ$ – $40^\circ$  latitude band. This can best be seen in Figure 4 (middle panel) which shows the zonal-mean RFs. The figure demonstrates the impact of latitude of  $\text{NO}_x$  emission on the global-mean net RF. The net RF for tropical emissions is around 7 times higher than that resulting from emissions in the  $60^\circ$ – $80^\circ$  bands in both hemispheres. Despite the global-mean short-lived ozone RFs being much higher for SH emissions (by more than a factor of 2 for the  $60^\circ$ – $80^\circ$  band), the same is not true for the net RFs, because the compensating methane and methane-induced  $\text{O}_3$  RFs are also larger for the SH emissions. Indeed, for the  $40^\circ$ – $60^\circ$  band, the net RF for the NH emissions is a factor of two larger than the corresponding SH case.

The latitudinal variation of the net RF is a complicated combination of different factors. As Figure 4 (bottom panel) shows, in the NH the methane lifetime change varies between low and high latitudes emissions by approximately a factor of six whereas for the short-lived ozone changes the variation is approximately a factor of three (the methane lifetime change per unit ozone change varies from about  $0.12$  to  $0.19$  yr  $\text{DU}^{-1}$ , a larger range than in the regional experiments). On this basis, it might be expected that the net RF would be *smaller* at low latitudes because the methane effect becomes larger – however this effect is compensated by the fact that the short-lived  $\text{O}_3$  RF per DU change approximately doubles from high to low latitudes, mostly because of the dependence of the RF on surface temperature. Figure 4 (middle panel) shows the much enhanced RF at low latitudes for the low latitude emission cases. Hence, the net RF is generally higher for lower latitude emissions cases.

## 5. Climate Emission Metrics

Radiative forcing provides an indication of the equilibrium climate effect of sustained  $\text{NO}_x$  emissions. Because of the differing lifetimes of the various components, RF does not give a useful view of the future impact of current emissions, which may be required for considering possible mitigation options and for comparison with other aviation climate impacts. We present values

for two climate metrics – the Global Warming Potential (GWP) and the Global Temperature Change Potential (GTP), following the methodology used in Myhre et al. (2011), which is identical to that in Fuglestvedt et al. (2010) apart from the inclusion of the effect of stratospheric water vapour changes due to methane changes.

As discussed in Fuglestvedt et al. (2010) there are many caveats and issues in defining and computing climate emission metrics. The GWP and GTP are presented here as they are the most widely discussed metrics. The GWP (with a hundred-year time horizon) is adopted for placing gases within the Kyoto Protocol on a common CO<sub>2</sub>-equivalent scale, and is the time-integrated RF due to a pulse emission of a gas, relative to a pulse emission of an equal mass of CO<sub>2</sub>. The GTP computes the temperature change at a given time (i.e. unlike the GWP it is not time-integrated), due to a pulse emission, relative to that from a pulse emission of an equal mass of CO<sub>2</sub>. The GTP could be more suitable for a target-based climate policy. GWPs are presented for the “traditional” time horizons (H) of 20, 100 and 500 years; the GTP is presented for H = 20, 50 and 100 years, which are more appropriate in a target-based context. As shown by Fuglestvedt et al. (2010) the NO<sub>x</sub> GTP is highly dependent on the choice of H. The GTP values are also sensitive to the choice of model used to represent heat uptake in the oceans and to the climate sensitivity. The calculations here assume an equilibrium climate sensitivity of 3.9 K for a CO<sub>2</sub> doubling.

Table 2 lists the specific RF values for the three components; these are used to generate the GWP and GTP values. Table 3 shows the total GWP and GTP for the three time horizons. The table in the supplementary information contains the individual components of these GWPs and GTPs.

Myhre et al. (2011) show considerable inter-model spread in the GWP and GTP values for present-day emissions; hence care is needed in applying the results from one model. In addition, because of the compensation between the different terms, the net metric values vary widely in both size and sign due to subtle changes in the individual components. For example, the GWP for H = 20, 100 and 500 year for the global emissions from the present-day fleet are 415, 75 and 23 respectively, which can be compared with the p-TOMCAT values in Myhre et al. (2011) of 218, -6.3 and -2.0. The individual components making up these net values differ (see Supplementary Information), however, by no more than 17% in the two studies.

Considering the GWP values, the values for emissions from China and India are similar for all H and several times larger than the values for emis-

sions from USA and Europe, with the global values intermediate between the two. This general pattern is supported by the latitudinal values (recall that these are for emissions near cruise altitude, rather than aviation emissions at all altitudes, and hence these are generally larger than the regional values), with a factor of 6 difference between the tropical and high latitude values. Values in the NH are generally higher than the SH, with some exceptions.

Stevenson and Derwent (2009) do not present detailed numerical values of their absolute 100-year GWP (AGWP) and so a detailed comparison is not possible. In contrast to our results, their net AGWP is almost always negative, irrespective of the location of emissions; in their model the impact on methane overwhelms the effect of the short-lived ozone forcing. Nevertheless, their net AGWP varies strongly with location, as in our study – their results are generally more negative for emissions in the tropics, with the most negative values in the central equatorial Pacific, because of the low background  $\text{NO}_x$  levels. Possible reasons for the difference in sign are discussed in the Conclusions.

The GWPs are uniformly positive for all cases presented here, but the GTP varies in sign from negative for  $H = 20$  and 50 years to positive for  $H = 100$  years. The fact that, for example,  $\text{GTP}(20)$  and  $\text{GWP}(20)$ , and the  $\text{GTP}(20)$  and  $\text{GTP}(100)$ , differ in sign, indicate the care necessary in metric choice for a given application. There is less clear differentiation in the GTP values for the regional experiments than was the case for the GWPs. The latitudinal experiments show more coherence. Unlike the GWPs, the peak GTP values are not for tropical emissions for two of the three time horizons, and the inter-hemispheric differences are more marked than in the GWP case. Although the metrics for lower latitude emissions are generally larger in magnitude than for higher latitude emissions, for  $\text{GTP}(20)$  and  $\text{GTP}(50)$  they are more effective at cooling, while for  $\text{GTP}(100)$  they are more effective at warming.

## 6. Conclusions

We have carried out chemical transport model experiments with regional perturbations to aircraft  $\text{NO}_x$  emissions. First emission perturbations were applied throughout the vertical extent of the atmosphere in four distinct geographical regions. Then  $\text{NO}_x$  was increased at cruise altitude in discrete latitude bands.

Our results show strong regional sensitivity of ozone and methane to changes in  $\text{NO}_x$ , particularly at cruise altitude. In general, low latitude emission increases result in stronger impacts on  $\text{O}_3$  column and  $\text{CH}_4$  lifetimes than higher latitudes emission increases. This is consistent with Grewe and Stenke (2008) and Stevenson and Derwent (2009). Within our four selected geographical regions, India exhibits the largest forcing sensitivity for the individual components to changes in aircraft  $\text{NO}_x$  emissions whereas Europe exhibits the smallest. This is in sharp contrast to the relative contribution from aircraft emissions to background  $\text{NO}_x$  levels in the UTLS region at these locations. Our experiments indicate that the latitude of the individual region is the dominant factor with regard to the net RF impact. We consider longitudinal variation in the  $\text{NO}_x$  impacts in only a limited way through our four regional experiments. Stevenson and Derwent (2009) show that there exists significant longitudinal variability in the time-integrated RF.

The SH ozone and methane is at all latitudes more sensitive to changes in  $\text{NO}_x$  than the corresponding northern latitudes. This can be explained by the variation in the  $\text{NO}_x$  background concentration. This is lower in the SH and hence an equally sized increase in  $\text{NO}_x$  emissions there results in a correspondingly larger impact. For lower latitudes perturbations the meridional extent of the composition change is much larger than higher latitudes perturbations where the change remains more confined to the region of perturbation. However, this sensitivity in  $\text{O}_3$  and  $\text{CH}_4$  change is not carried over to the net RF, which is much more symmetric about the equator.

The GWP and GTP also show a strong latitudinal dependence but illustrate the strong dependence on the metric choice and the choice of time horizon. For the GWP, the effect of  $\text{NO}_x$  emissions is always positive, for all time horizons, with values for low latitude emissions at cruise levels typically 6–8 times higher than for high latitude emissions. By contrast, the GTP changes sign from cooling to warming between time horizons of 50 and 100 years (as was also found in some cases in Fuglestvedt et al. (2010)).

A serious issue is that available calculations of climate metrics for aviation  $\text{NO}_x$  emissions do not agree even on the sign of the net effect (Stevenson and Derwent, 2009; Fuglestvedt et al., 2010; Myhre et al., 2011). Because of the strong compensation between the positive RF from the short-lived ozone changes, and the negative RF from the methane and methane-induced ozone change, even small differences in the individual values can have large impacts on the net RF, GWP and GTP. These differences persist even when the same radiative transfer code is used (e.g. Myhre et al., 2011), indicating

the differences are most likely related to the chemical response of the models. Holmes et al. (2011) noted that there are two distinct issues: those which are specific to the model response to aviation emissions (e.g. the ozone change per unit emission) and more general model responses (e.g. the ozone change per unit change in methane). Myhre et al. (2011) pointed out that much of the model spread in the net RF appeared to be related to inter-model differences in the change in methane lifetime per unit ozone change. In the regional experiments presented here, this quantity was surprisingly invariant. It may be that this factor is driving the difference in signs of the GWP between our results and those in Stevenson and Derwent (2009); it is of note that even given the strong compensation in the RF terms, the GWPs are always positive here, irrespective of location of emissions, and in Stevenson and Derwent (2009) the GWP are almost always negative irrespective of location, indicating some robustness of the response within a single model.

As the impact of a given amount of  $\text{NO}_x$  is dependent on the background concentration the accurate simulation of  $\text{NO}_x$  in the model may also be necessary. This remains difficult to achieve and inter-model differences can be large (e.g. Brunner et al., 2003). Important factors in attempting to achieve a realistic representation of background  $\text{NO}_x$  are the use of up-to-date surface emissions and a reliable representation of convective uplift from surface emissions and  $\text{NO}_x$  emissions from lightning (Berntsen and Isaksen, 1999).

#### *Acknowledgments*

We are grateful to the AERO2k and QUANTIFY community for providing access to emissions data. GR acknowledges funding through the EU FP6 QUANTIFY Project. MOK acknowledges funding from NERC through the AIM Project. KS acknowledges support from the EU FP7 ECLIPSE project. We are grateful to O. Dessens for engaging discussions and to three reviewers for many helpful comments.

#### **References**

van Aardenne, J., Dentener, F., Olivier, J., Peters, J., Ganzeveld, L., 2005. The EDGAR3.2 Fast Track 2000 data set (32FT2000). Joint Research Center, Institute for Environment and Sustainability, Climate Change Unit, Ispra, Italy.

- ACI, 2011. ACI Global Traffic Forecast 2010–2029. Airports Council International, Montreal, Canada. <http://www.aci.aero/publications>.
- Airbus, 2010. Global Market Forecast 2010–2029. Airbus HQ, 1 Rond Point Maurice Bellonte, 31707 Blagnac Cedex, France. <http://www.airbus.com/company/market/gmf2010>.
- Atkinson, R.A., Baulch, D.L., Cox, R.A., Crowley, J.N., Jr., R.F.H., Hynes, R.G., Jenkin, M.E., Kerr, J.A., Rossi, M.J., Troe, J., 2005. Summary of evaluated kinetic and photochemical data for atmospheric chemistry, <http://www.iupac-kinetic.ch.cam.ac.uk/>, web version.
- Berntsen, T.K., Fuglestvedt, J.S., Joshi, M.M., Shine, K.P., Stuber, N., Ponater, M., Sausen, R., Hauglustaine, D.A., Li, L., 2005. Response of climate to regional emissions of ozone precursors: sensitivities and warming potentials. *Tellus 57B*, 283–304, doi:10.1111/j.1600-0889.2005.00152.x.
- Berntsen, T.K., Isaksen, I.S.A., 1999. Effects of lightning and convection on changes in tropospheric ozone due to NO<sub>x</sub> emissions from aircraft. *Tellus 51B*, 766–788, doi:10.1034/j.1600-0889.1999.t01-3-00003.x.
- Boeing, 2010. Current Market Outlook 2010–2029. Boeing Commercial Airplanes, Market Analysis, P. O. Box 3707 MC 21-28, Seattle, WA 98124-2207, USA. <http://www.boeing.com/cmo>.
- Borken, J., Steller, H., 2006. Report on the Draft Emission Inventories for Road Transport in the year 2000. Technical Report. Deutsches Institut für Luft- und Raumfahrt (DLR), Institut für Verkehrsforschung.
- Brunner, D., Staehelin, J., Rogers, H.L., Köhler, M.O., Pyle, J.A., Hauglustaine, D., Jourdain, L., Berntsen, T.K., Gauss, M., Isaksen, I.S.A., Meijer, E., van Velthoven, P., Pitari, G., Mancini, E., Grewe, V., Sausen, R., 2003. An evaluation of the performance of chemistry transport models by comparison with research aircraft observations. Part 1: Concepts and overall model performance. *Atmospheric Chemistry and Physics 3*, 1609–1631, doi:10.5194/acp-3-1609-2003.
- Cook, P.A., Savage, N.H., Turquety, S., Carver, G.D., O'Connor, F.M., Heckel, A., Stewart, D., Whalley, L.K., Parker, A.E., Schlager, H., Singh, H.B., Avery, M.A., Sachse, G.W., Brune, W., Richter, A., Burrows, J.P.,

- Purvis, R., Lewis, A.C., Reeves, C.E., Monks, P.S., Levine, J.G., Pyle, J.A., 2007. Forest fire plumes over the North Atlantic: p-TOMCAT model simulations with aircraft and satellite measurements from the ITOP/ICARTT campaign. *Journal of Geophysical Research* 112, D10S43, doi:10.1029/2006JD007563.
- Derwent, R.G., Stevenson, D.S., Doherty, R.M., Collins, W.J., Sanderson, M.G., Johnson, C.E., 2008. Radiative forcing from surface NO<sub>x</sub> emissions: Spatial and seasonal variations. *Climatic Change* 88, 385–401, doi:10.1007/s10584-007-9383-8.
- Edwards, J.M., Slingo, A., 1996. Studies with a flexible new radiation code.1. Choosing a configuration for a large-scale model. *Quarterly Journal of the Royal Meteorological Society* 122A, 689–719, doi:10.1002/qj.49712253107.
- Endresen, Ø., Sørgård, E., Behrens, H.L., Brett, P.O., Isaksen, I.S.A., 2007. A historical reconstruction of ships' fuel consumption and emissions. *Journal of Geophysical Research* 112, D12301, doi:10.1029/2006JD007630.
- Eyers, C.J., Norman, P., Middel, J., Plohr, M., Michot, S., Atkinson, K., Christou, R., 2005. AERO2k global aviation emissions inventories for 2002 and 2025. Version 1.1, Report No. QinetiQ/04/01113, QinetiQ, Farnborough, Hampshire, U. K.
- Fuglestedt, J.S., Berntsen, T.K., Isaksen, I.S.A., Mao, H., Liang, X.Z., Wang, W.C., 1999. Climatic forcing of nitrogen oxides through changes in tropospheric ozone and methane; global 3D model studies. *Atmospheric Environment* 33, 961–977, doi:10.1016/S1352-2310(98)00217-9.
- Fuglestedt, J.S., Shine, K.P., Berntsen, T., Cook, J., Lee, D.S., Stenke, A., Skeie, R.B., Velders, G.J.M., Waitz, I.A., 2010. Transport impacts on atmosphere and climate: Metrics. *Atmospheric Environment* 44, 4648–4677, doi:10.1016/j.atmosenv.2009.04.044.
- Grewe, V., Stenke, A., 2008. AirClim: an efficient tool for climate evaluation of aircraft technology. *Atmospheric Chemistry and Physics* 8, 4621–4639, doi:10.5194/acp-8-4621-2008.
- Grewe, V., Tsati, E., Hoor, P., 2010. On the attribution of contributions of atmospheric trace gases to emissions in atmospheric model applications. *Geoscientific Model Development* 3, 487–499, doi:10.5194/gmd-3-487-2010.

- Henderson, B.H., Pinder, R.W., Crooks, J., Cohen, R.C., Hutzell, W.T., Sarwar, G., Goliff, W.S., Stockwell, W.R., Fahr, A., Mathur, R., Carlton, A.G., Vizuete, W., 2011. Evaluation of simulated photochemical partitioning of oxidized nitrogen in the upper troposphere. *Atmospheric Chemistry and Physics* 11, 275–291, doi:10.5194/acp-11-275-2011.
- Holmes, C.D., Tang, Q., Prather, M.J., 2011. Uncertainties in climate assessment for the case of aviation NO. *Proceedings of the National Academy of Sciences* 108, 10,997–11,002, doi:10.1073/pnas.1101458108.
- Holtlag, A.A.M., Boville, B.A., 1993. Local versus nonlocal boundary-layer diffusion in a global climate model. *Journal of Climate* 6, 1825–1825.
- Hoor, P., Borken-Kleefeld, J., Caro, D., Dessens, O., Endresen, O., Gauss, M., Grewe, V., Hauglustaine, D., Isaksen, I.S.A., Jöckel, P., Lelieveld, J., Myhre, G., Meijer, E., Olivie, D., Prather, M., Poberaj, C.S., Shine, K.P., Staehelin, J., Tang, Q., van Aardenne, J., van Velthoven, P., Sausen, R., 2009. The impact of traffic emissions on atmospheric ozone and OH: results from QUANTIFY. *Atmospheric Chemistry and Physics* 9, 3113–3136, doi:10.5194/acp-9-3113-2009.
- Hoyle, C.R., Marécal, V., Russo, M.R., Allen, G., Arteta, J., Chemel, C., Chipperfield, M.P., D’Amato, F., Dessens, O., Feng, W., Hamilton, J.F., Harris, N.R.P., Hosking, J.S., Lewis, A.C., Morgenstern, O., Peter, T., Pyle, J.A., Reddman, T., Richards, N.A.D., Telford, P.J., Tian, W., Viciani, S., Volz-Thomas, A., Wild, O., Yang, X., Zeng, G., 2011. Representation of tropical deep convection in atmospheric models – Part 2: Tracer transport. *Atmospheric Chemistry and Physics* 11, 8103–8131, doi:10.5194/acp-11-8103-2011.
- Jaeglé, L., Jacob, D.J., Brune, W.H., Tan, D., Faloon, I.C., Weinheimer, A.J., Ridley, B.A., Campos, T.L., Sachse, G.W., 1998a. Sources of HO<sub>x</sub> and production of ozone in the upper troposphere over the United States. *Geophysical Research Letters* 25, 1709–1712, doi:10.1029/98GL00041.
- JPL, 2003. Chemical kinetics and photochemical data for use in atmospheric studies. Evaluation number 14, JPL publication 02-25.
- Kärcher, B., 1996. Aircraft-generated aerosols and visible contrails. *Geophysical Research Letters* 23, 1933–1936, doi:10.1029/96GL01853.

- Köhler, M.O., Rädcl, G., Dessens, O., Shine, K.P., Rogers, H.L., Wild, O., Pyle, J.A., 2008. Impact of perturbations to nitrogen oxide emissions from global aviation. *Journal of Geophysical Research* 113, D11305, doi:10.1029/2007JD009140.
- Lee, D.S., Pitari, G., Grewe, V., Gierens, K., Penner, J.E., Petzold, A., Prather, M.J., Schumann, U., Bais, A., Bernsten, T., Iachetti, D., Lim, L., Sausen, R., 2010. Transport impacts on atmosphere and climate: Aviation. *Atmospheric Environment* 44, 4678–4734, doi:10.1016/j.atmosenv.2009.06.005.
- Meijer, E.W., Van Velthoven, P.F.J., Wauben, W.M.F., Beck, J.P., Velders, G.J.M., 1997. The effects of the conversion of nitrogen oxides in aircraft exhaust plumes in global models. *Geophysical Research Letters* 24, 3013–3016, doi:10.1029/97GL53156.
- Myhre, G., Shine, K.P., Rädcl, G., Gauss, M., Isaksen, I.S.A., Tang, Q., Prather, M.J., Williams, J.E., van Velthoven, P., Dessens, O., Koffi, B., Szopa, S., Hoor, P., Grewe, V., Borken-Kleefeld, J., Bernsten, T.K., Fuglestvedt, J.S., 2011. Radiative forcing due to changes in ozone and methane caused by the transport sector. *Atmospheric Environment* 45, 387–394, doi:10.1016/j.atmosenv.2010.10.001.
- Olivier, J.G.J., Aardenne, J.A.V., Dentener, F.J., Pagliari, V., Ganzeveld, L.N., Peters, J.A.H.W., 2005. Recent trends in global greenhouse gas emissions: regional trends and spatial distribution of key sources. *Environmental Sciences* 2, 81–99, doi:10.1080/15693430500400345.
- Pitari, G., Mancini, E., Bregman, A., 2002. Climate forcing of subsonic aviation: Indirect role of sulfate particles via heterogeneous chemistry. *Geophysical Research Letters* 29, 2057, doi:10.1029/2002GL015705.
- Prather, M.J., 1986. Numerical advection by conservation of second-order moments. *Journal of Geophysical Research* 91, 6671–6681, doi:10.1029/JD091iD06p06671.
- Ramanathan, V., Dickinson, R.E., 1979. The role of stratospheric ozone in the zonal and seasonal radiative energy balance of the earth-troposphere system. *Journal of the Atmospheric Sciences* 36, 1084–1104.

- Rossow, W.B., Schiffer, R.A., 1991. ISCCP cloud data products. *Bulletin of the American Meteorological Society* 72, 2–20.
- Savage, N.H., Law, K.S., Pyle, J.A., Richter, A., Nüß, H., Burrows, J.P., 2004. Using gome NO<sub>2</sub> satellite data to examine regional differences in tomcat model performance. *Atmospheric Chemistry and Physics* 4, 1895–1912, doi:10.5194/acp-4-1895-2004.
- Schwartz Dallara, E., Kroo, I.M., Waitz, I.A., 2011. Metric for comparing lifetime average climate impact of aircraft. *AIAA Journal* 49, 1600–1613, doi:10.2514/1.J050763.
- Stevenson, D.S., Derwent, R.G., 2009. Does the location of aircraft nitrogen oxide emissions affect their climate impact? *Geophysical Research Letters* 36, L17810, doi:10.1029/2009GL039422.
- Stockwell, D.Z., Giannakopoulos, C., Plantevin, P.H., Carver, G.D., Chipperfield, M.P., Law, K.S., Pyle, J.A., Shallcross, D.E., Wang, K.Y., 1999. Modelling NO<sub>x</sub> from lightning and its impact on global chemical fields. *Atmospheric Environment* 33, 4477–4493, doi:10.1016/S1352-2310(99)00190-9.
- Tiedtke, M., 1989. A comprehensive mass flux scheme for cumulus parameterization in large-scale models. *Monthly Weather Review* 117, 1779–1800.
- Wang, Z.S., Chien, C.J., Tonnesen, G.S., 2009. Development of a tagged species source apportionment algorithm to characterize three-dimensional transport and transformation of precursors and secondary pollutants. *Journal of Geophysical Research* 114, D21206, doi:10.1029/2008JD010846.

Table 1: Description of regional domain properties and change in composition. The fourth column shows the contribution from unperturbed aircraft emissions (base case) to  $\text{NO}_2$  at cruise altitude within the respective domain. The scaling factor (column 5) is applied to aircraft emissions in each grid cell in the domain. The  $\text{NO}_x$  emissions are perturbed by  $0.036 \text{ Tg (N)}$  per year in each case and the corresponding global ozone changes are expressed in DU (column 6).

Region	Geographical Extent	Surface Area ( $\text{km}^2$ )	$\Delta \text{NO}_2$ due to aircraft (%)	Scaling factor (%)	$\Delta \text{O}_3$ (DU)
1 USA	$126^\circ\text{W}$ – $64^\circ\text{W}$ ; $23^\circ\text{N}$ – $50^\circ\text{N}$	$1.65 \cdot 10^7$	44.6	20	0.022
2 Europe	$14^\circ\text{W}$ – $40^\circ\text{E}$ ; $35^\circ\text{N}$ – $71^\circ\text{N}$	$1.32 \cdot 10^7$	58.1	28	0.018
3 India	$65^\circ\text{E}$ – $91^\circ\text{E}$ ; $6^\circ\text{N}$ – $33^\circ\text{N}$	$8.11 \cdot 10^6$	13.6	260	0.041
4 China	$96^\circ\text{E}$ – $126^\circ\text{E}$ ; $18^\circ\text{N}$ – $44^\circ\text{N}$	$8.47 \cdot 10^6$	30.1	108	0.038

Table 2: Steady-state radiative forcings (in  $\text{mW m}^{-2} (\text{Tg (N) yr}^{-1})^{-1}$ ) and global methane lifetime change (in years  $(\text{Tg (N) yr}^{-1})^{-1}$ ) with applied feedback factor for sustained aircraft  $\text{NO}_x$  emissions by the present-day global fleet, constant percentage increases in aviation emissions at all altitudes in four regions and for near-cruise altitude emission increases at various latitudes (see text for details).

	Short-lived $\text{O}_3$ forcing	$\text{CH}_4$ -induced $\text{O}_3$ forcing	$\text{CH}_4$ forcing	Net $\text{NO}_x$ forcing	$\text{CH}_4$ lifetime change
Global	28.8	-6.03	-16.5	6.25	-0.172
USA	20.1	-4.76	-13.0	2.33	-0.136
Europe	13.7	-3.08	-8.44	2.17	-0.0878
India	45.6	-8.81	-24.1	12.6	-0.251
China	40.8	-7.08	-19.4	14.3	-0.202
60–80° N	18.4	-2.96	-8.11	7.34	-0.0843
40–60° N	24.5	-4.26	-11.7	8.55	-0.121
20–40° N	52.6	-9.81	-26.8	16.0	-0.279
0–20° N	124	-19.1	-52.4	52.2	-0.544
0–20° S	132	-22.3	-61.0	48.3	-0.634
20–40° S	65.8	-15.4	-42.1	8.25	-0.438
40–60° S	42.1	-10.3	-28.2	3.60	-0.293
60–80° S	39.5	-8.90	-24.4	6.19	-0.253

Table 3: Global Warming Potentials (GWP) and Global Temperature change Potentials (GTP) for emissions by the present-day global fleet, constant percentage increases in aviation emissions at all altitudes in four regions and for near-cruise altitude emission increases at various latitudes. GWP values for one-year pulse emissions of  $\text{NO}_x$  for a 20, 100 and 500 year time horizons and GTP values for 20, 50 and 100 years. All values are on a per kg (N) basis and are relative to  $\text{CO}_2$ . The GTP values are specific to a given value of climate sensitivity (see text for details).

	GWP			GTP		
	H=20	H=100	H=500	H=20	H=50	H=100
Global	415	75	23	-239	-56	8.6
USA	222	29	8.9	-222	-49	2.6
Europe	171	27	8.1	-135	-31	2.7
India	749	151	46	-304	-75	18
China	769	169	51	-191	-52	22
60–80° N	376	86	26	-63	-19	11
40–60° N	460	101	31	-116	-31	13
20–40° N	909	189	57	-315	-79	24
0–20° N	2640	614	187	-345	-113	80
0–20° S	2567	572	174	-562	-157	73
20–40° S	747	104	31	-708	-158	9.5
40–60° S	421	47	14	-499	-110	3.2
60–80° S	489	76	23	-392	-89	7.8

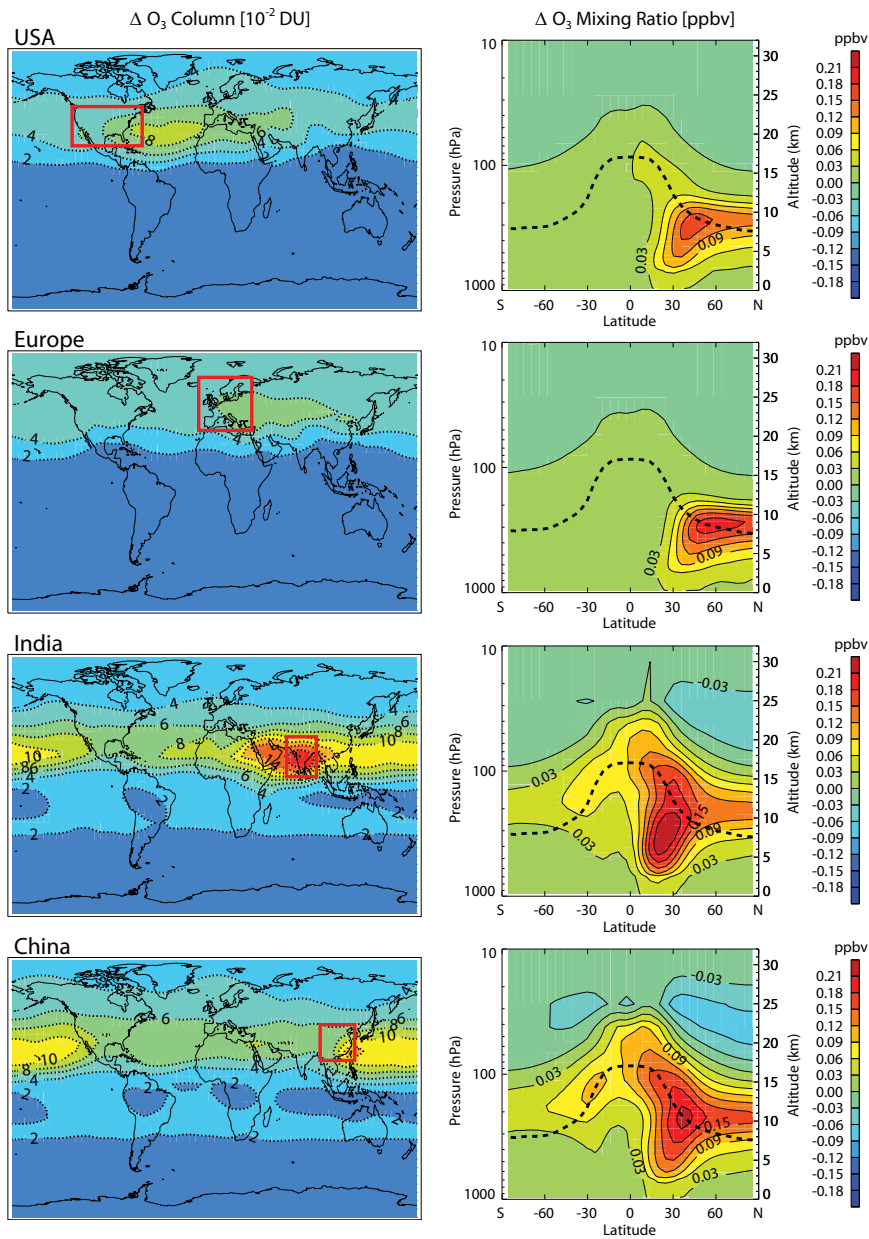


Figure 1: Annual mean O<sub>3</sub> changes calculated by the p-TOMCAT model for aircraft NO<sub>x</sub> emission increases by 0.036 Tg (N) per year in four geographical regions. Figures on the left show the change in vertical O<sub>3</sub> column ( $10^{-2}$  DU). The extent of the area with increased emissions is indicated by a red rectangle for each region. Figures on the right show the change in zonal mean O<sub>3</sub> volume mixing ratio (ppbv), the dashed line indicates the location of the tropopause.

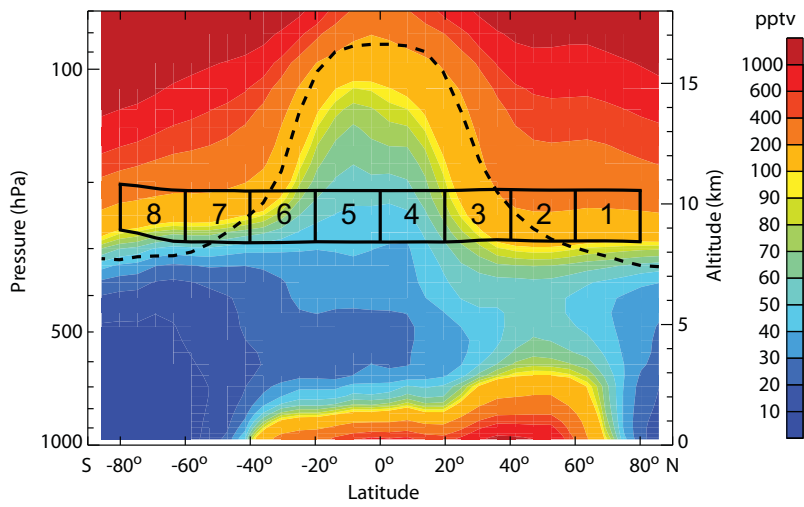


Figure 2: Colour shading shows the zonally averaged annual-mean  $\text{NO}_x$  ( $= \text{NO} + \text{NO}_2$ ) mixing ratios in the p-TOMCAT model for the year 2002. The numbered boxes indicate cross-sections through the eight latitude bands where emissions were increased. The dashed line represents the annual mean position of the tropopause.

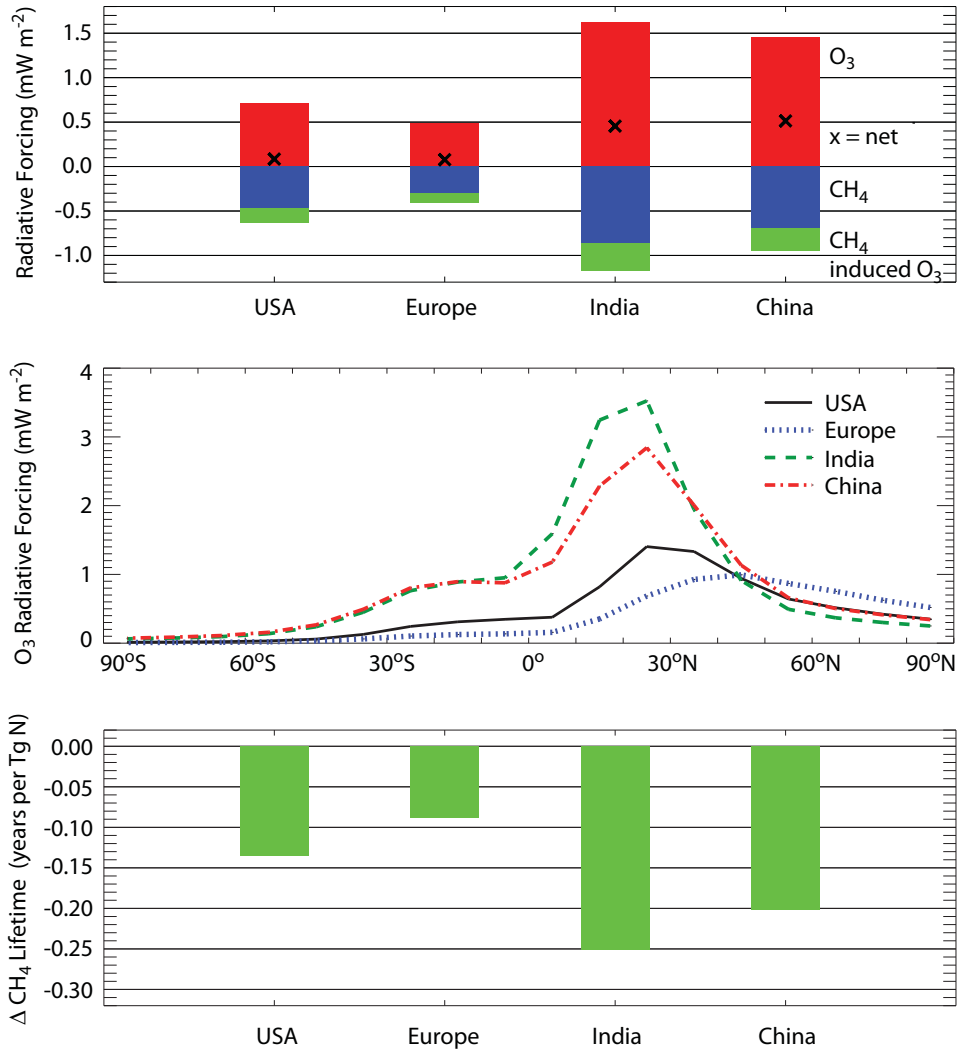


Figure 3: Top panel: Global-mean radiative forcing in  $\text{mW m}^{-2}$  due to a regional increase of aircraft  $\text{NO}_x$  emissions of  $0.036 \text{ Tg (N)}$  per year. Net radiative forcing (black cross) is shown for emission increases over the USA, Europe, India and China as well as the different contributions to it due to short-lived ozone production (red), the reduction of methane lifetime (blue) and the methane-induced ozone decrease (green). Middle panel: Zonal dependence of the short-lived ozone radiative forcing for the four regional experiments: USA (solid), Europe (dotted), India (dashed), China (dash-dotted). Bottom panel: Change in  $\text{CH}_4$  lifetime in years per  $\text{Tg (N)}$ .

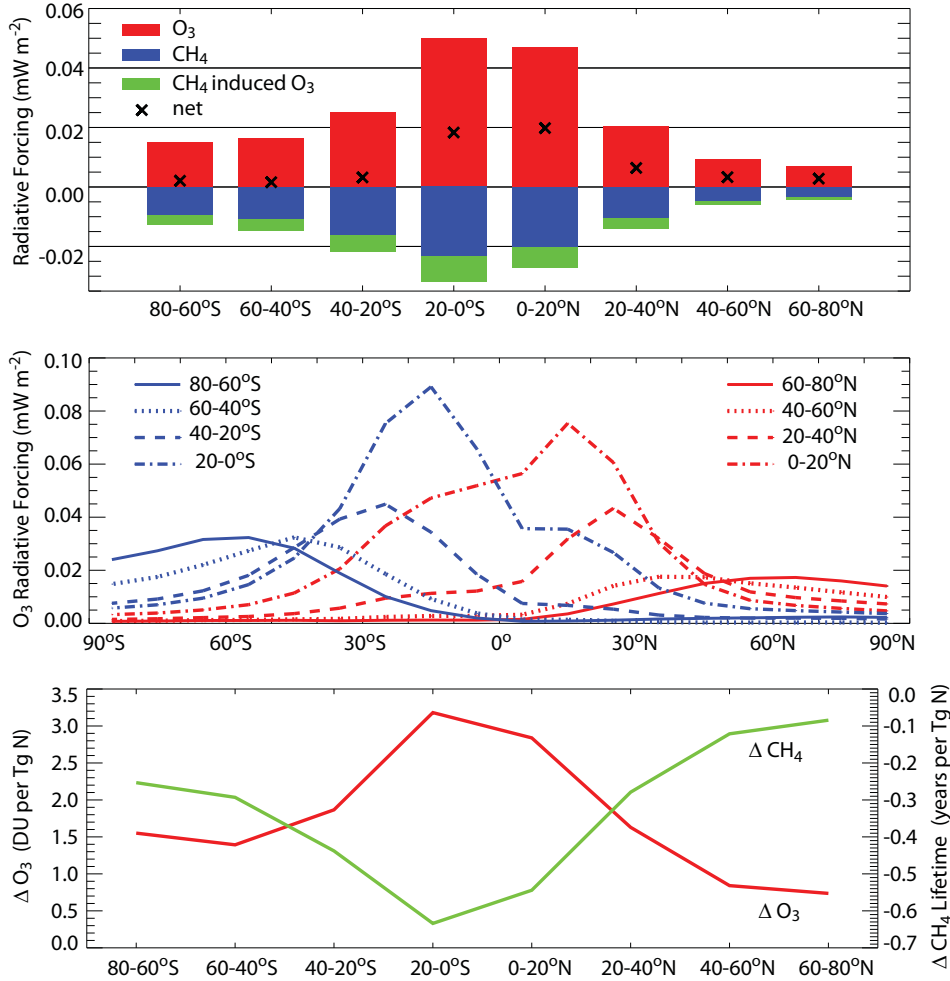


Figure 4: Response to an increase of  $\text{NO}_x$  emissions by  $3.8 \cdot 10^{-4} \text{ Tg (N)}$  per year at cruise altitude in 20 degree wide latitude bands. Top panel: Shows the net global-mean radiative forcing (black cross) in  $\text{mW m}^{-2}$  as well as the different contributions to it due to short-lived ozone production (red), the reduction of methane lifetime (blue) and the methane-induced ozone decrease (green). Middle panel: Zonal dependence of the short-lived ozone radiative forcing for the same latitude bands as shown in top panel. Bottom panel: Global mean change in O<sub>3</sub> column (red, in DU) and CH<sub>4</sub> lifetime (green, in years per Tg (N) per year).

## Supplementary Information: Full Climate Metrics Data

This supplementary section contains the full version of Table 3 in the manuscript. It shows Global Warming Potentials (GWP) and Global Temperature change Potentials (GTP) for emissions by the present-day global aircraft fleet, constant percentage increases in aviation emissions at all altitudes in four regions and for near-cruise altitude emission increases at various latitudes. It includes the individual components that make up the total values. (Note that in the corresponding table (Table 5) in Myhre et al. (2011)<sup>1</sup>, the component values for the methane and methane-induced ozone forcings for the GTP were inadvertently transposed.) (a) GWP values for one-year pulse emissions of NO<sub>x</sub> for a 20, 100 and 500 year time horizons and (b) GTP values for 20, 50 and 100 years. The first three numbers show the individual contributions from the short-lived O<sub>3</sub>, the CH<sub>4</sub>-induced O<sub>3</sub> and the CH<sub>4</sub> (which includes stratospheric water vapour changes), respectively; the net GWP and GTP are shown in bold. All numbers are rounded, so that the net values may not be the sum of numbers as they are presented here. All values are on a per kg (N) basis and are relative to CO<sub>2</sub>. The GTP values are specific to a given value of climate sensitivity (see text in Section 5 of the manuscript for details).

(a) GWP	H=20	H=100	H=500
Global	1170–193–558 = <b>415</b>	331–66–190 = <b>75</b>	101–20–58 = <b>23</b>
USA	814–152–434 = <b>222</b>	231–52–150 = <b>29</b>	70–16–46 = <b>8.9</b>
Europe	555–99–286 = <b>171</b>	158–34–97 = <b>27</b>	48–10–30 = <b>8.1</b>
India	1850–282–815 = <b>749</b>	525–97–277 = <b>151</b>	159–29–84 = <b>46</b>
China	1652–227–656 = <b>769</b>	470–78–223 = <b>169</b>	143–24–68 = <b>51</b>
60–80° N	745–95–274 = <b>376</b>	212–33–93 = <b>86</b>	64–9.9–28 = <b>26</b>
40–60° N	992–136–396 = <b>460</b>	282–47–135 = <b>101</b>	86–14–41 = <b>31</b>
20–40° N	2130–314–907 = <b>909</b>	605–108–308 = <b>189</b>	184–33–94 = <b>57</b>
0–20° N	5020–611–1770 = <b>2640</b>	1430–210–603 = <b>614</b>	434–64–183 = <b>187</b>
0–20° S	5340–714–2064 = <b>2567</b>	1520–245–702 = <b>572</b>	462–75–213 = <b>174</b>
20–40° S	2660–493–1420 = <b>747</b>	757–169–484 = <b>104</b>	230–51–147 = <b>31</b>
40–60° S	1700–330–954 = <b>421</b>	485–113–325 = <b>47</b>	147–34–99 = <b>14</b>
60–80° S	1600–285–825 = <b>489</b>	455–98–281 = <b>76</b>	138–30–85 = <b>23</b>
(b) GTP	H=20	H=50	H=100
Global	368–160–447 = <b>-239</b>	57–30–83 = <b>-56</b>	47–9.9–28 = <b>8.6</b>
USA	257–126–353 = <b>-222</b>	40–24–66 = <b>-49</b>	33–7.9–22 = <b>2.6</b>
Europe	175–82–228 = <b>-135</b>	27–15–43 = <b>-31</b>	22–5.1–15 = <b>2.7</b>
India	582–233–653 = <b>-304</b>	91–44–122 = <b>-75</b>	74–15–42 = <b>18</b>
China	521–188–525 = <b>-191</b>	81–35–98 = <b>-52</b>	67–12–33 = <b>22</b>
60–80° N	235–79–220 = <b>-63</b>	37–15–41 = <b>-19</b>	30–4.9–14 = <b>11</b>
40–60° N	312–113–316 = <b>-116</b>	49–21–59 = <b>-31</b>	40–7.0–20 = <b>13</b>
20–40° N	672–260–727 = <b>-315</b>	105–49–136 = <b>-79</b>	86–16–46 = <b>24</b>
0–20° N	1580–507–142 = <b>-345</b>	246–95–264 = <b>-113</b>	202–32–90 = <b>80</b>
0–20° S	1680–590–1650 = <b>-562</b>	262–111–308 = <b>-157</b>	215–37–105 = <b>73</b>
20–40° S	840–408–1140 = <b>-708</b>	131–76–213 = <b>-158</b>	107–25–73 = <b>9.5</b>
40–60° S	537–273–763 = <b>-499</b>	84–51–142 = <b>-110</b>	69–17–49 = <b>3.2</b>
60–80° S	368–236–660 = <b>-392</b>	79–44–123 = <b>-89</b>	64–15–42 = <b>7.8</b>

<sup>1</sup>Myhre, G., et al. (2011) Radiative forcing due to changes in ozone and methane caused by the transport sector, *Atmos. Environ.* 45(2), 387–394, doi:10.1016/j.atmosenv.2010.10.001.